

Suture-free laser-assisted vessel repair using CO₂ laser and liquid albumin solder

Ingrid C. D. Y. M. Wolf-de Jonge

Academic Medical Center
Department of Vascular Surgery
Meibergdreef 9
1105 AZ Amsterdam, The Netherlands

Michal Heger

Academic Medical Center
Laser Center and Department of Experimental Surgery
Meibergdreef 9
1105 AZ Amsterdam, The Netherlands

Jan van Marle

Academic Medical Center
Department of Cell Biology and Histology
Meibergdreef 9
1105 AZ Amsterdam, The Netherlands

Ron Balm

Academic Medical Center
Department of Vascular Surgery
Meibergdreef 9
1105 AZ Amsterdam, The Netherlands

Johan F. Beek

Academic Medical Center
Laser Center
Meibergdreef 9
1105 AZ Amsterdam, The Netherlands

1 Introduction

Laser welding is progressively being accepted as a suitable alternative to conventional suturing in a wide range of (micro)surgical applications.¹⁻⁵ In the vascular field, the technique is predominantly being pursued for laser-assisted vascular anastomosis (LAVA) and laser-assisted vascular repair (LAVR). Both procedures share the ultimate objective of sealing the vascular lumen from the perivascular environment by creating an inter-/intravascular coaptation capable of resisting systolic pressures well above malignant hypertensive values (>180 mmHg)⁶ without compromising vascular patency or causing sequelae (intimal hyperplasia, aneurysms).⁷⁻¹³ Compared to conventional microsuture anastomosis, several advantages have been demonstrated, including reduction of foreign body reactions and inflammation, liquid-tight seals, faster healing, and the prospect of simpler vessel repair for minimally invasive procedures. Laparoscopic conventional suturing is often difficult and associated with a long learning curve. The nontactile technique of LAVA/R can therefore

Abstract. Numerous studies have shown that the use of proteinic solders during laser-assisted vascular anastomosis (LAVA) and repair (LAVR) can significantly increase welding strength, but these studies combined solder-mediated LAVA/R with the use of stay sutures, thereby defeating its purpose. In an *in vitro* study, we examined the leaking point pressures (LPPs) and histological damage profile of porcine carotid arteries following albumin solder-mediated CO₂ LAVR without the use of sutures. Longitudinal arteriotomies (9.1 ± 0.8 mm in length) were sheathed with 25% liquid bovine serum albumin solder, and LAVR was performed using a micromanipulator-controlled CO₂ laser operating at 170-mW power and 1.25-mm spot size in continuous wave mode. The welding regime consisted of a transversal zigzag pass followed by one or two longitudinal zigzag passes, producing an irradiance of 13.9 W/cm² and energies of 10.5 J and 11.3 J per mm weld, respectively. LPPs were measured by the fluid infusion technique, and histological analysis was performed with light, fluorescence, and polarization microscopy. The LPP of the two-pass welds was 351 ± 158 mmHg versus 538 ± 155 mmHg for the three-pass welds. Thermal damage was confined primarily to the adventitial layers, with limited heat diffusion into the media below the solder around the coaptation interface. © 2008 Society of Photo-Optical Instrumentation Engineers. [DOI: 10.1117/1.2953531]

Keywords: tissue welding; vascular anastomosis; carotid artery; collagen; fluorescence microscopy; thermal damage analysis.

Paper 07140R received Apr. 17, 2007; revised manuscript received Dec. 14, 2007; accepted for publication Feb. 12, 2008; published online Jul. 28, 2008.

provide a viable solution for laparoscopic use. In areas other than vascular surgery, its feasibility has already been proven in animal experiments.¹⁴

In an effort to optimize welding outcomes by limiting tissue damage to a restricted perimeter while enhancing welding strength, numerous laser systems have been explored, often in conjunction with chromophore-spiked proteinic or biomaterial solders.¹ The use of solders offers several important advantages over the use of native tissue as a conjugation surface. In addition to being superior ligature material,^{15,16} the solders act as wavelength-specific heat sinks, confining thermal damage primarily to the regions of chromophore-amplified localized energy absorption. Secondly, solders aid in the alignment of opposing vessel edges in that they act as weak glues,¹² thereby partially compensating for the absence of stay sutures. The manipulability of protein (and chromophore) concentration further allows for controllable and optimizable welding protocols, which is imperative for standardizing treatment parameters.

Despite the abundance of CO₂ LAVA/R articles, equivalent to the number of research years invested in this field, we found only three reports on solder (fibrin glue)-mediated CO₂

Address all correspondence to: Michal Heger, Department of Experimental Surgery, Academic Medical Center, Meibergdreef 9, 1105 AZ Amsterdam, The Netherlands. Tel: 31 20 5666653; Fax: +31 20 6976621; E-mail: M.Heger@amc.uva.nl

LAVA.¹⁵⁻¹⁷ Grubbs et al.¹⁵ clearly demonstrated that the CO₂ laser-solder combination yielded significantly better results when compared to conventional LAVA. However, stay sutures were used in all three studies for optimal alignment of the vessel edges, which defeats the clinical purpose of the procedure (e.g., prevention of foreign body reactions). The limited number of reports on solder-CO₂ LAVA/R is somewhat surprising, given the beneficial thermodynamics of CO₂ laser-tissue interactions in relation to the clinically expedient damage profile. At 10.6- μ m wavelength, the main absorber is water. The high water content in the vessel wall (in conjunction with the aqueous solder solvent) accounts for predominant photon deposition in the adventitia and possibly superior media, resulting in shallow heat confinement at the proper irradiation time. Such an inherently effective quarantine of thermal damage allows the vessel wall to retain its structural integrity and viability and leaves the endothelial layer intact. In light of the promising results presented by Grubbs et al., this study examined the leaking point pressures (LPPs) and the histological characteristics of solder-tissue fusion following *in vitro* LAVR of porcine carotid arteriotomies in the presence of bovine serum albumin (BSA) solder and the absence of stay sutures.

2 Materials and Methods

2.1 Solder and Tissue Preparation

The solder solution was prepared by dissolving 25% (w/v) BSA (Fraction V, Sigma Aldrich, St. Louis, Missouri) in deionized water. Porcine carotid arteries (external diameter 0.5 to 0.6 cm) were harvested from euthanized animals that had undergone different surgical procedures. After sectioning the arteries into 4-cm segments, the perivascular tissue was trimmed and the specimens were submerged in histidine-tryptophan-ketoglutarate preservative solution (Custodiol, Tramedico, Weesp, The Netherlands). Both the solder solution and the vascular segments were stored in the dark at 4 °C until further use for up to 20 days. For histological investigations, vascular samples were stored for a maximum of 4 days. A longitudinal arteriotomy was created with a scalpel and scissors, and its length was measured with a digital caliper. Prior to LAVR, the opposing mural ends were aligned with tweezers without the use of stay sutures, after which 15 μ L of solder was distributed uniformly over the incision site with a pipette.

2.2 Laser

A 10.6- μ m CO₂ laser (UltraPulse 5000C, Coherent, Santa Clara, California) with a low-power 632.8-nm aiming beam was focused onto the vessel through the microscope optics of a joystick micromanipulator-controlled operating microscope (6 \times objective, OpMi-1, Carl Zeiss, Oberkochen, Germany). The laser was operated in continuous wave (CW) mode at a mean \pm SD power of 170 \pm 1 mW (Ophir Optronics, Jerusalem, Israel), corresponding to a mean \pm SD irradiance of 13.9 \pm 0.1 W/cm² at a 1.25-mm-diameter spot size. The spot size was measured by irradiating photosensitive paper (Kodak, Rochester, New York) at the predefined working distance and laser parameters. Spots were measured under a stereomicroscope with a calibrated ruler. The exposure duration

was controlled with a foot switch and timed manually using a stopwatch. The laser beam was passed over the incision in a raster scanning (zigzag) manner. The first pass was administered transversely over the adjoined vessel edges, with an approximate distance of 3.8 mm between the outer boundaries of the irradiation area. For the second and, in some cases, third pass, the laser was moved longitudinally along and over the anastomosis at approximately the same speed as during the first pass. The total dwell time was calculated as the cumulative exposure time of individual, sequential passes. Complete desiccation of the solder, as assessed microscopically, marked the end point of laser irradiation. The incised segments were subjected to two ($n=19$) or three ($n=11$) laser passes depending on the subjective judgment of solder desiccation.

2.3 Leaking Point Pressure

The leaking point pressure (LPP) was measured directly after laser irradiation (two passes: $n=15$; three passes: $n=5$) in accordance with the method of Basu et al.¹⁸ and Fahner et al.¹⁹ One end of the laser-treated carotid segment was sealed by ligation and the vessel lumen filled with methylene blue dye (Sigma-Aldrich). The other end was ligated around a blunt 25G needle that was connected to a rate-controlled syringe infusion pump and a pressure controller (Braun Medical, Melsungen, Germany) through an interposed T-valve. For online pressure recording, the pressure controller was coupled to a pressure transducer (Baxter Healthcare, Deerfield, Illinois) that transmitted the digitized output signals to a PC workstation.

Upon complete submersion of the artery in a 0.9% saline bath, the intraluminal pressure was gradually raised by the infusion of additional dye at 99 mL/h. The LPP was defined as the pressure at which leakage of methylene blue through the weld was observed, accompanied by a simultaneous drop in pressure.

2.4 Histological Analysis

Following LAVR, the vessel segments ($n=10$) were fixed in 4% buffered formaldehyde for 8 h and paraffinized. The paraffin-embedded samples were cut into 5- μ m-thick cross-sections and stained with hematoxylin-eosin (H&E) according to standard protocol ($n=36$).²⁰ For the acquisition of bright-field images, a Leica DMBL microscope equipped with a Leica DC200 CCD camera and customized software was used (Leica Microsystems, Wetzlar, Germany). For fluorescence analysis, the samples were visualized under a fluorescence microscope (Eclipse E600, Nikon, Bunnik, The Netherlands) at the following settings: $\lambda_{ex}=535 \pm 25$ nm, 565-nm dichroic mirror, $\lambda_{em}=590$ nm cuton (G-2A filter set). Samples were assessed for wall-to-wall alignment and solder attachment. Proper alignment was achieved when the margins of the intima and adventitia at the incisional interface displayed a relatively uninterrupted, coalescent geometrical continuity. The level of solder attachment was evaluated qualitatively based on the degree of physical connectivity between solder and the adventitia/media. The extent of thermal damage was assessed histologically by means of histopathological markers such as the degree of eosinophilia and basophilia of matrix components (collagen and elastin) and nuclei, respectively. To cor-

roborate histopathology, microscopic analysis was performed using a Zeiss polarization microscope equipped with linear polarizers (a fixed polarizer and an adjustable analyzer) and a first-order (full range) retardation plate to enhance the contrast between birefringent material (intact collagen and elastin) and material that had lost its birefringence (thermally denatured collagen and elastin).

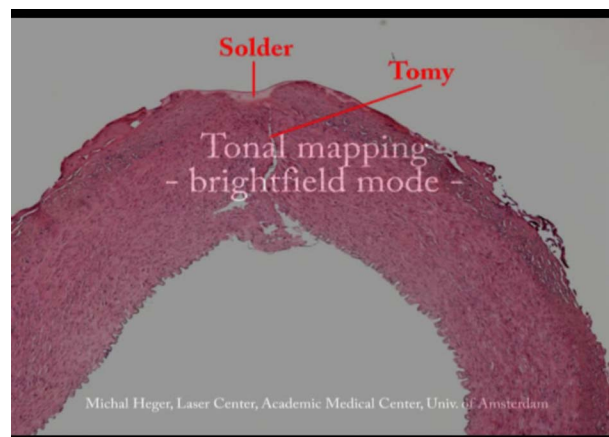
2.5 Software-Assisted Histological Analysis

In addition to visual assessment, histopathology was qualified by software-assisted image analysis. Our method for damage determination is based on two foundational premises: (1) the generation of supracritical temperatures imparts distinctive histopathological characteristics on thermally affected tissue; and (2) a positive correlation exists between the degree of laser-induced matrix and cellular damage and the extent of basophilicity/eosinophilicity (i.e., tonal gradients in H&E staining patterns). Denaturation of matrix proteins such as collagen and elastin depends on the distribution of isotherms as a function of time following laser irradiation. Inasmuch as the histochemical reaction relies on the exposed binding sites for the mordant/dye, the degree of luminance of the hue is proportional to the level of protein denaturation. The so-called residual thermal damage profile in the vessel wall, stretching from the nucleation centers (severely thermally affected matrix regions) to the distal boundaries of heat diffusion (moderately affected regions), therefore displays a histological grading from hyper— to mild eosinophilia, respectively.^{21–23} Consequently, qualitative and semi-quantitative analyses can be performed on the basis of differences in tonality. Similar principles apply at the cellular level, where the nuclei of thermally afflicted cells exhibit hyperchromatic basophilia and the cytoplasm stains are increasingly eosinophilic.^{22,24,25} With image analysis software (Adobe Photoshop 7.0), it is possible to generate (iso)tonal maps by tuning the tonal cutoff and tonal range without altering color balances in the RGB spectrum. This type of analysis can be performed on both brightfield as well as fluorescence images, given the quasi-stoichiometric rate of eosin binding to (denatured) elastin/collagen and the proportional intensity of fluorescence emission.

The method consisted of gradually narrowing the tonal range of the unedited RGB image of the cross section by increments of 2 on a scale of 0 to 255 (representing tints and shades, respectively), thereby increasing the luminance cutoff until only deeply shaded pixels (hue-specific grayscale values of 0 to 3) remained visible. The image at every incremental step was saved separately. No additional editing tools were used. Video 1 shows a single histological cross section that was compiled to demonstrate the analytical principles and outcomes of the dynamic tonal mapping technique in brightfield and fluorescence modes. The sequence of consecutive frames was interlaced to compose the video at a frame rate of 25/s (Adobe Premiere Pro 1.5).

2.6 Statistical Analysis

Statistical Package for Social Sciences software (SPSS, Chicago, Illinois) was used to calculate means, standard deviations, and correlation coefficients. Kolmogorov-Smirnov and Shapiro-Wilks tests were performed to determine the normality of the distribution of LPPs in the two and three laser



Video 1 Illustration of the software-assisted image analysis technique. (Iso)tonal maps were generated by tuning the tonal cutoff and tonal range without altering color balances in the RGB spectrum. The tonal range of the unedited RGB image was narrowed by increments of 2 on a scale of 0 to 255 (representing tints and shades, respectively), thereby increasing the luminance cutoff until only deeply shaded pixels (hue-specific grayscale values of 0 to 3) remained visible. These are representative of intensely stained tissue segments, which correspond to segments that had likely undergone relatively more thermal damage. Arrowheads represent severely damaged perivascular tissue and/or solder (MPG, 4.87 MB). [URL: <http://dx.doi.org/10.1117/1.2953531.1>].

passes groups. Both tests indicated a normal distribution of the two-pass group ($P=0.138$ and 0.155 , respectively, when the outlier at 813 mmHg was omitted from the Shapiro-Wilks test) and the three-pass group ($P=0.178$ and 0.087 , respectively). An unpaired two-tailed Student's *t*-test (assuming equal variances) was performed to determine the significance of the differences between mean LPPs.

3 Results

Arteriotomies of a mean length of 9.1 ± 0.8 mm were homogeneously sheathed with $15 \mu\text{L}$ BSA solder and lased with two or three passes until the solder appeared completely desiccated. The mean \pm SD cumulative dwell time was 573 ± 43 s/repair with a mean dwell time of 261 ± 40 s/pass, corresponding to mean incident energies of 97 ± 7 and 44 ± 7 J, respectively, and a cumulative energy of 10.7 J/mm weld and a total energy density of 243.5 ± 18.4 J/cm² (total irradiated area of ~ 0.4 cm² per weld) when the two- and three-pass regimes are grouped. For the two-pass regime only, the mean \pm SD cumulative dwell time was 562 ± 41 s/repair with a mean dwell time of 281 ± 21 s/pass, corresponding to mean incident energies of 96 ± 7 and 48 ± 4 J, respectively, and a cumulative energy of 10.5 J/mm weld and a total energy density of 221.3 ± 17.6 J/cm². For the three-pass regime, the mean \pm SD cumulative dwell time was 606 ± 34 s/repair with a mean dwell time of 202 ± 11 s/pass, corresponding to mean incident energies of 103 ± 6 and 34 ± 2 J, respectively, and a cumulative energy of 11.3 J/mm weld and a total energy density of 243.3 ± 14.3 J/cm².

3.1 Leaking Point Pressures

Figure 1 depicts the LPP values of laser-welded arteriotomies classified according to LPP range. The mean \pm SD LPP was

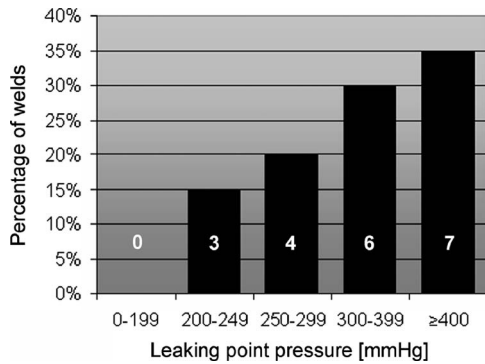


Fig. 1 Leaking point pressures (LPPs) after CO₂-laser-assisted vascular repair of porcine carotid arteries ($n=20$) plotted as a function of LPP category. Suture-free longitudinal arteriotomies were subjected to two or three laser passes in the presence of bovine serum albumin solder. The numbers in the bars indicate the quantity of vessels per LPP category.

398 ± 174 mmHg over a range of 202 to 813 mmHg. Eighty-five percent (17 out of 20) of welds had an LPP ≥ 250 mmHg. The mean LPP of the two-pass welds was 351 ± 158 mmHg versus 538 ± 155 mmHg for the three-pass welds ($P=0.034$). No correlation was found between LPP and either length of arteriotomy or carotid/solder age.

3.2 Histological Analysis—Light and Polarization Microscopy

Microscopically, three out of ten cross-sectioned samples exhibited severed vessel wall ends, which had probably occurred during histological preparation, and were excluded from analysis. Of the remaining seven samples, four (57%) were properly aligned at the intima and adventitia, exhibiting a continuous geometry at the incision site. Three wall-to-wall welds did not coalesce confluent at the luminal boundaries but displayed a relatively congruous alignment at the adventitial level [Fig. 2(a)]. All evaluated samples were primarily coated at the solder-tissue interface, with no or only mar-

ginal direct wall-to-wall fusion. Direct wall-to-wall attachment occurred most proximal to the solder weld [Fig. 2(b)].

Laser-induced damage was assessed based on distinct histopathological features of the irradiated carotid sections. Thermal damage in the form of protein denaturation extended laterally over varying distances on either side of the incision as evidenced by the hyperchromatic H&E staining pattern [Fig. 2(a)]. The mean breadth of the laterally extending thermal damage zone was 1.8 mm. The occasional presence of vacuoles in the solder suggests that temperatures crossed the vaporization threshold of water (>100 °C). However, the absence of carbonization or charring rules out a detrimental sustenance of supracritical temperatures and consequential desiccation of the irradiated tissue layers. Moreover, the thickness of thermally damaged adventitia was approximately identical to the thickness of contralateral, unaffected adventitia, corroborating the finding that LAVR did not cause any notable tissue shrinkage or excessive water evaporation. The damage in depth was chiefly restricted to the adventitia, although some supracritical heat diffusion into the media did occur. Thermal damage to the media, based on the differential staining intensities of the matrix components by eosin [Fig. 2(b), arrows] and nuclei by hematoxylin [Fig. 2(b), arrowhead], was predominantly confined to areas adjacent to the incision and to the direct vicinity of the solder. Areas showing thermal damage were associated with an altered birefringence (Fig. 3).

3.3 Histological Analysis—Fluorescence Microscopy

Excitation of H&E tissue samples with green light induces emission of fluorescence in the orange spectrum by eosin.^{26,27} The (H&E) stain can hence be used to fluorescently label acidophilic components such as elastin and, to a lesser degree, collagen so as to provide additional structural information to conventional histology. In addition, the staining intensities can be differentiated more easily, which can contribute to the accuracy of histopathological analysis (see Video 2). The attachment of solder to mural tissue seems to be unimpaired across the entire solder-tissue interface toward both extralat-

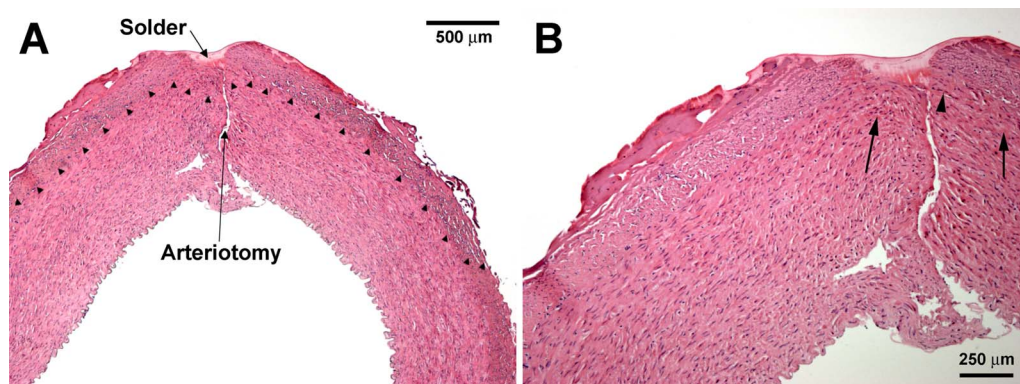


Fig. 2 Histological section of a 4-day-old, 9.4-mm incised carotid artery segment that was subjected to three CO₂ laser passes with a total dwell time of 625 s and a cumulative energy of 11 J/mm weld. (a) The thermal damage zone is delineated with arrowheads. Note that the apposed vessel wall edges are coated primarily at the solder-tissue interface, with only little direct laser-induced tissue fusion immediately below the solder. Hematoxylin-eosin, magnification 10 \times . (b) Higher magnification of (a), with focus on the solder-tissue interface and the arteriotomy. Thermal damage is histopathologically characterized by hypereosinophilia (arrows), marking the denaturation of matrix proteins such as elastin and collagen, and hyperbasophilia (arrowhead), signifying damaged or overactive nuclei. Magnification 20 \times .

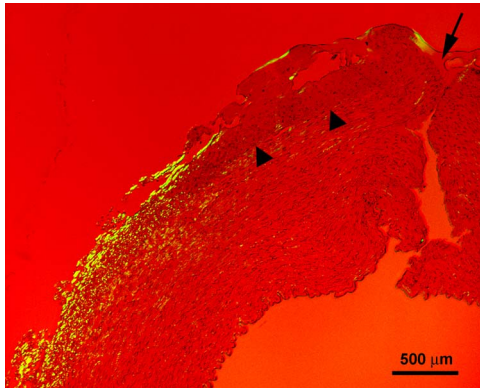
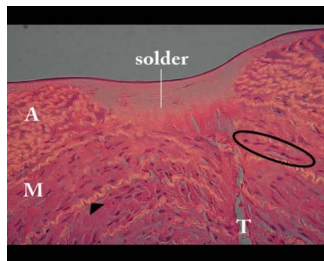


Fig. 3 Polarization microscopy image taken of a 4-day-old, 9.2-mm incised carotid segment that was subjected to two laser passes with a total dwell time of 545 s and a cumulative energy of 10 J/mm weld. The general (redness) of the slide, which is due to the first-order retardation plate positioned between the sample and the analyzer, corresponds to regions with no birefringence (i.e., glass coverslip). The arrowheads indicate the boundary between the *tunica adventitia* and the media, while the arrow points to the solder. Note that regions in the direct vicinity of the solder and lateral extensions exhibit an altered birefringence as a result of laser-induced thermal damage. Birefringence is retained at a distance of approximately 1 mm from the incision. Vacuolization in the solder suggests that vaporization has occurred. Polarization of light passing through the media is absent, probably due to the orientation of the elastin and collagen fibers. Hematoxylin-eosin, magnification 12 \times . (Color online only.)

eral ends [Fig. 4], and involves the adventitia as well as the upper media, as evidenced by the unequivocal demarcation of these layers based on the striation pattern and elastin density. Furthermore, the solder appears to have been thermally fixed to the elastic fibrils in the adventitia as well as the media. A more intense fluorescence emission by the matrix components of the media immediately beneath the solder (Fig. 4, arrow) confirms that the tissue in this region has been thermally afflicted. Interestingly, damage to the media prevailed only in regions situated in the vicinity of the solder, and not so much in more remote subadventitial regions.



Video 2 A video has been compiled to illustrate the contribution of fluorescence images to brightfield images. By gradually changing the opacity of two superimposed images (with starting opacities of 0% and 100%) in opposite directions (from 0 to 100% and from 100 to 0%), one can get a good impression of the additive value of the fluorescence image in juxtaposition to the brightfield image. Several structural features and the extent of thermal damage become better accentuated. A=adventitia, M=media, T=arteriotomy, circled area=cell nuclei, arrowhead=elastin fiber (MPG, 2.88 MB). [URL: <http://dx.doi.org/10.1117/1.2953531.2>].

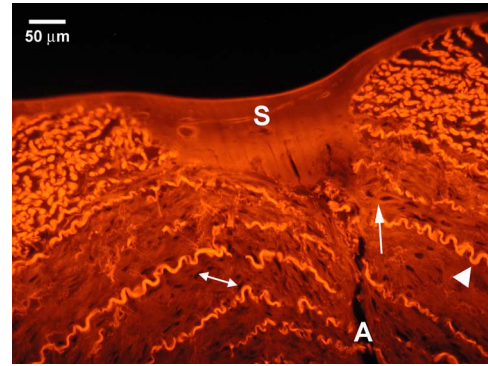


Fig. 4 Fluorescence image of the solder-tissue interfacial region of the welded artery shown in Fig. 2. The hyperfluorescent striae (arrowhead) are elastic fibrils in the adventitia (densely, longitudinally striated) and media (dispersely, transversely striated). The background fluorescence emanates from mural collagen and albumin in the solder (S). Note that the relative fluorescence intensity is greater directly below the solder (arrow). The double arrow points to black spaces that correspond to nuclei. A=arteriotomy. Hematoxylin-eosin, $\lambda_{\text{ex}} = 535 \pm 25$ nm, 565-nm dichroic mirror, $\lambda_{\text{em}} = 590$ nm cuton. Magnification 80 \times .

3.4 Software-Assisted Histological Analysis

Figure 5 is a regressive tonal map compilation of an H&E-stained cross section in brightfield 5(a)–5(d) and fluorescence modes 5(e)–5(h), i.e., the tonal range is gradually narrowed to improve visual acuity and to facilitate more objective interpretation of histological damage. The specimen portrayed in the brightfield sequence stems from a 4-day-old, 9.2-mm incised carotid segment that was subjected to two laser passes with a total dwell time of 545 s. The intensely staining zone below the solder around the incision [Fig. 5(d), between the lines] contains a relatively high density of hyperchromatic nuclei. In Fig. 5(d), where only the darkest pixels are visualized (corresponding to anatomical loci with most severe damage/metabolic activity), some nuclei in the tunica media in close proximity to the incision remain visible (encircled),

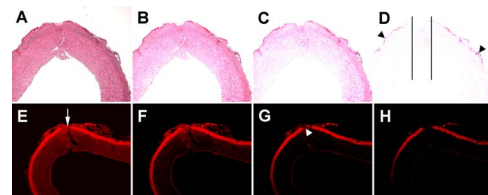


Fig. 5 Regressive tonal map sequences of hematoxylin-eosin-stained cross sections that had undergone LAVR. Panels (a) to (d), taken from a 4-day-old, 9.2-mm incised carotid segment that was subjected to two laser passes with a total dwell time of 545 s, are brightfield images in tonal ranges of 0 to 255 (a), 0 to 175 (b), 0 to 135 (c), and 0 to 75 (d). The space between the lines in panel (d) roughly demarcates the region with the most profound thermal damage. Residual hyperchromatic staining is clearly visualized in the demarcated area. The arrowheads point to undissected perivascular tissue that has been severely afflicted by laser irradiation. Panels (e) to (h), taken from a 4-day old, 9.4-mm incised carotid artery irradiated with three passes for 625 s, are fluorescence images in tonal ranges 0 to 255 (e), 0 to 195 (f), 0 to 115 (g), and 0 to 15 (h). The arrow in (e) indicates the solder, and the arrowhead in (g) points to thermally affected media that was folded upward during apposition.

suggesting that heat diffusion in depth was more profound at the subsolder interfacial region than at laterally more-distal medial regions. This was the case in all sampled histological sections. It should be emphasized, however, that the nuclear hyperchromatism cannot be unequivocally attributed to thermally induced necrosis per se, since mechanical damage, preservation time (up to 4 days in histidine-tryptophan-ketoglutarate), and an inherently high cellular metabolism in smooth muscle cells may contribute to or entirely account for the observed staining profile. Nevertheless, the apparent indication that these loci are situated in a zone with the highest cumulative energy deposition, and not in adjacent tissue, is meaningful and should not be dismissed. The arrowheads in Fig. 5(d) indicate excessive thermal damage to undissected perivascular tissue where substantial nucleation has taken place, affecting both matrix constituents and cells.

The cross section exhibited in fluorescence mode [Figs. 5(e)–5(h)], was taken from a 4-day-old, 9.4-mm tomied carotid artery irradiated with three passes for 625 s. Due to the high affinity for eosin by elastin, a clear anatomical delineation can be made between the media and the elastin-rich adventitia. The position of the solder is indicated [Fig. 5(e), arrow], as well as the proximal area that has suffered substantial thermal denaturation [Fig. 5(g), arrowhead]. Again, major affliction to the media is located around the solder and the coaptation, although the depth of the damage appears to be more superficial than in the two-pass vascular segment [Figs. 5(a)–5(d)]. This is likely due to different thermal damage thresholds of cells versus elastin and collagen, insofar as the former are more susceptible to heat.²² Moreover, signal acquisition at this magnification (20×) is dominated by emission from elastin-bound eosin and, to a lesser extent, from collagen-bound eosin. These proteins are more densely disseminated than cells. What is also noteworthy is the gradual shading of adventitia at both distal ends of the solder as the tonal range is narrowed, implying a relatively broad area of superficial thermal affliction. The outer bounds have experienced the least incident energy due to the Gaussian profile of the beam, whereby the tapered decline in fluorescence intensity with narrowing tonal range reflects damage as a result of heat diffusion.

4 Discussion

The status quo of LAVA/R is that several important outcome parameters need to be optimized for laser-based modalities to become unequivocally advantageous over conventional suturing. A foremost parameter is the strength of the weld and its gradual decline over time, which to date has been inferior to sutured coaptations.¹ Consequently, dehiscence and aneurysm formation at the welding site have a more frequent occurrence in LAVA/R cases compared to conventional microsuturing techniques.^{15,28,29} Furthermore, confinement of thermal damage is crucial inasmuch as excessive denaturation of cellular and matrix components in the vessel wall could compromise its postoperative integrity and patency.⁵ The extent of thermal damage is strongly dependent on how laser dosimetry (irradiance, pulse duration, and pulsing pattern) is attuned to the spectral properties of the target chromophore(s). Since thermal damage is exponentially related to temperature and linearly related to time of exposure,³⁰ an optimal balance

between laser parameters, pulsing regime, and these spectral properties must be established *a priori* so as to achieve substantial welding strengths while deterring nonselective damage.

With a $\sim 300\text{-cm}^{-1}$ absorption coefficient of water at 10.6- μm wavelength³¹ and an optical penetration depth of approximately 13 to 20 μm ,^{5,12} the CO₂ laser is ideal for superficial tissue denaturation and thus confinement of nonselective damage. As a result, numerous tissue welding studies have been conducted with this laser system, producing positive results over a broad range of applications, but also revealing its critical drawbacks, particularly with respect to LAVA/R.^{1,5} Ironically, the shallow thermal damage zone created by the CO₂ laser simultaneously constitutes a major disadvantage in that it is associated with reduced bond strength. Since thermal denaturation does not extend over the full coaptation depth, the bursting pressure threshold relies on a small, superficial volume of cross-linked matrix proteins.⁵ This could be alleviated through longer irradiation times, but the resulting “tissue contraction, cell death, and weakening of the bond” due to excessive heat diffusion preclude CO₂ LAVA/R from yielding viable and reliable clinical outcomes, at least according to Bass and Treat.⁵ Nevertheless, it is our belief that the full clinical potential of solder-mediated CO₂ LAVA/R is yet to be reached through the expansion/optimization of the rudimentary approach presented here. In several small pilots that preceded this study, we experimented with different parameters, including different pulse durations (1 to 3 s), pass speeds, and powers. Although the optimal parameters were chosen based on preliminary results, further optimization is by no means excluded, particularly with respect to pass speed.

Several studies on CO₂ LAVA^{15,16,32} have reported significant increases in welding strength when the laser procedure is carried out in combination with a proteinic solder such as fibrin glue^{15–17} (versus native tissue as bonding material). However, stay sutures were employed in all cases to secure the anastomosis, which undoubtedly contributed to the outcomes in regard to welding strength and a reduction in aneurysm incidence but violated the principles behind LAVA. In this study, liquid BSA solder-mediated LAVR was therefore carried out in the absence of sutures using a bimodal laser pass regime (a transverse zigzag pass followed by one or two longitudinal zigzag passes), producing LPPs of 351 ± 158 and 538 ± 155 mmHg with the two and three cumulative passes, respectively, without inflicting extensive thermal damage to the media. These results compare favorably when juxtaposed to sutured LAVA/R LPP values reported in the literature (Fig. 6): the three-pass regime produced the second-to-highest mean LPP outcome published to date for the CO₂ laser and competes easily with LPP values reported for different laser systems,¹ while the two-pass regime yielded LPPs well above malignant hypertensive values. Interestingly, the results were obtained with irradiances that were at most 15% of those applied in comparable studies and energies/mm weld that were at least 200% greater^{15,16,18,33–38} (Fig. 6) while using a relatively low solder protein concentration in liquid form.^{12,13}

The relatively high LPP values likely resulted from a combination of factors. First, solder-mediated welding strength enhancements correlate positively to the effective coagulation

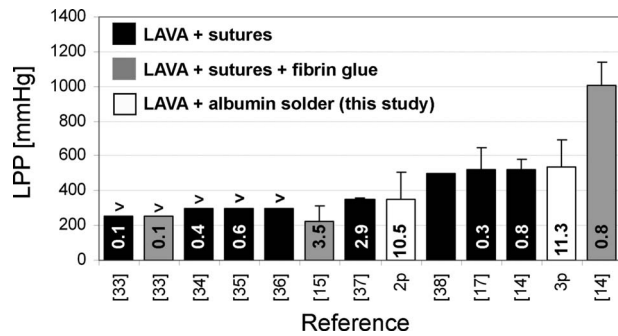


Fig. 6 Comparative summary of leaking point pressure (LPP) values following CO₂ LAVA/R. The LPP values are plotted for each study (reference number in brackets) published to date on this subject matter. The bars with a > sign represent studies in which the assayed vessels were capable of withstanding the designated pressure. Specific LPPs were not measured in these studies. The black bars correspond to suture-assisted LAVA/R without solder, the gray bars correspond to studies in which suture-assisted LAVA/R was performed in the presence of fibrin glue solder, and the white bars correspond to this study, in which sutureless, solder-mediated LAVA/R was performed. (The numbers on the x axis for these two bars represent the number of passes employed during welding.) The values inside the bars represent energies per mm weld (J/mm) used in the respective study. The data for these calculations were either obtained from the publication (e.g., the laser parameters and welding protocol) or extrapolated using data from the literature on the average diameter of the welded veins/arteries and coronary circumference/length of the weld. Missing values stem from insufficient information to perform calculations.

area,³³ i.e., the area of physical connectivity between adjoined tissue segments. When the coagulation area expands laterally over the adventitia in the presence of a solder, it provides effectively more molecular anchor points than would be the case for LAVA/R without solder.^{18,34–39} This is illustrated in Fig. 4, where the BSA appears to be uninterruptedly tethered to collagen and the longitudinally oriented elastin fibers in the adventitia as well as the transversely oriented elastin fibers in the media, stretching outward in a seemingly consistent pattern. At lower magnification (Fig. 2), it becomes evident that the widely spanning laser-induced interactions between BSA and collagen/elastin are chiefly responsible for the vascular resilience, inasmuch as the opposing tissue edges are, for the largest part, not coapted. It should be noted that, although the coaptation area is rather substantial as a result of the zigzag pass regime [Fig. 2(a)], it is difficult to extrapolate to what extent the outer flanks of solder-tissue fusion contribute to the overall welding strength. Irradiated liquid solders tend to rupture at the solder midline when tension is applied (see the following paragraph), suggesting that the welding strength is governed by interactions between albumin molecules rather than by albumin-collagen/elastin interactions. In the case of liquid solders, the outward coagulative spread may therefore be less pertinent than for semisolid solders, in which the cross-linked albumin can withstand greater forces in the solder than at the interface.

Second, for vessel welding modalities that rely on superficial damage profiles, such as CO₂ LAVA/R, the degree of cross-linking between the mural proteins (if applicable), the solder proteins, and at the solder-tissue interface becomes equally important, if not paramount, for achieving clinically

respectable welding strengths. Apparently, optimal cross-linking and coronary welding strengths are dependent on (1) the proximity of participating protein molecules and (2) the thermodynamic evolution during and following laser irradiation. The former has been eloquently demonstrated by McNally et al.,^{12,13} who have proven that higher protein concentrations in the solder (i.e., greater intermolecular proximity) result in more robust welds. The authors further noted that solid solders tend to rupture at the solder-tissue interface, whereas liquid solders of equal protein concentration do so roughly at the solder midline. This implicitly underscores the importance of intermolecular proximity, inasmuch as solid solders, although malleable, conform less optimally to the tissue surface in comparison to liquid solders and therefore may not be in complete contact with the tissue. In our experiments, a liquid 25% (w/v) BSA solution was applied to the arteriotomies, which, in light of our results and the results reported in Refs. 12 and 13, partly justifies the relatively high LPPs but concomitantly leaves room for significant improvements. (McNally et al.¹³ reported an average increase in tensile strength of 166% when increasing BSA concentration from 25% to 60%.)

The influence of thermodynamic evolution during and after laser irradiation on welding strength is exemplified by the low irradiances and high energies/mm weld used as well as the differential LPP values generated by the two-pass versus the three-pass regime. Figure 6 shows that the energy deposition per mm weld is significantly greater compared to other studies, whereas the irradiance is much smaller due to the large spot size at comparable power. This means that a relatively sizable amount of energy is applied to the weld, but in a manner in which its spatial as well as temporal distribution preclude the generation of supracritical temperatures (little or no histological evidence of thermal damage to the media) while ensuring proper cross-linking (high LPPs). The laser parameters, in conjunction with the pass regime, therefore must have accounted for effective heat diffusion and/or the generation of optimal temperatures at the solder-tissue interface. Although an unequivocal explanation for these results remains at large, some answers may be derived from the fact that optimum welding strength is strongly correlated to an optimum temperature at which cross-linking takes place.^{12,40} In controlled experiments, Lemole et al.⁴¹ have demonstrated that tensile strengths of water bath-heated apposed bovine tendons peaked at 62 °C, corresponding to the experimentally derived temperature range of collagen denaturation,⁴² and fell sharply at temperatures exceeding 65 °C, which was accompanied by notable denaturation and shrinkage of the tissue. According to the authors, the “peaking effect” may be ascribed to a properly sustained fibrillar orientation of collagen in which optimal intermolecular, noncovalent (re)bonding is facilitated. At supracritical temperatures (>65 °C), longer sequences of H-bonds break, and the native triple-helical structure of collagen transits to a lower-energy, random coiled (shrunken) state⁴² in which the orientation of the fibrils likely precludes optimum bonding in the context of welding strengths. In the presence of a BSA solder, the kinetics become even more complex in that protein demixing must occur for coaptations to form, which requires that both proteins must possess similar isothermal unfolding characteristics. Coincidentally, the denaturation temperature of serum albu-

min is ~ 67 °C for BSA¹² and ~ 64 °C for its human analog.⁴³ Moreover, using electron microscopy, McNally et al.¹² have found that BSA is able to “diffuse” into the collagen matrix and intertwine into extracellular matrices at solder-tissue interfacial temperatures of ~ 68 °C, whereas at increasing temperatures, the diffusion/intertwining diminished or completely disappeared. Taken altogether, these findings suggest that optimal cross-linking conditions between collagen fibrils as well as between collagen and albumin molecules are centered around the threshold temperatures for denaturation. With temperature being an exponential entity in Arrhenius models of thermal damage, selection of proper laser parameters and pulsing regime in light of the preceding becomes absolutely crucial for successful welding outcomes. Given the high LPPs, it is thus not unlikely that the thermal profiles created with our lasing protocol conformed, albeit to an extent, to ideal conditions at the solder-tissue interface.

In our opinion, for welding of various tissues, visual feedback is an adequate method to obtain good results. Consequently, a next step in optimizing CO₂ LAVA/R, besides the use of strength-enforcing biodegradable scaffolds, would be the use of a temperature-controlled fiber-optic CO₂ laser system. Katzir and others (including researchers from our group in an earlier study on welding of intestine) have used, tested, and optimized this temperature-controlled laser system. It has proven its worth for welding of a wide variety of tissues and applications, including safe dural defect reconstruction and laparoscopic repair, which further demonstrated the safety of the system.^{44–46}

In conclusion, a sutureless, solder-mediated CO₂ LAVA modality has been presented. Essentially, the two most important parameters of LAVA/R have been improved: a minimally invasive (sutureless) increase in welding strength and a reduction of thermal necrosis, particularly in the media. Much emphasis has been placed on the role of the welding area, the importance of intermolecular proximity of solder/matrix proteins, and the decisively imperative temperature isotherms at the solder-tissue interface in the context of cross-linking kinetics of collagen, albumin, and possibly other matrix proteins such as elastin. Fortunately, these factors leave much room for improvement of the modality, e.g., through higher solder protein concentrations,^{12–14} selection of a solder protein that better matches the denaturation temperature of collagen (e.g., human serum albumin),⁴³ or by introducing additional procedures, such as immediate rapid cooling after laser irradiation⁴¹ by means of, for example, spurts of cryogen. On a fundamental level, issues such as multiple overlapping passes and the exact contribution of the extent of the welded area on LPPs will need to be resolved to further optimize the modality. Naturally, aneurysm formation will have to be assessed. In any case, CO₂ LAVA/R does harness the potential of clinical applicability in light of these results, and warrants further research into its possibilities as well as limitations as a treatment modality.

Acknowledgments

This work was supported by the Technological Collaboration Grant (TSGE 1048) of the Dutch Ministry of Economic Affairs. We thank Raphaella Kerindongo for the histological preparations.

References

1. I. C. Wolf-de Jonge, J. F. Beek, and R. Balm, “25 years of laser assisted vascular anastomosis (LAVA): what have we learned?” *Eur. J. Vasc. Endovasc Surg.* **27**, 466–476 (2004).
2. M. Talmor, C. B. Bleustein, and D. P. Poppas, “Laser tissue welding: a biotechnological advance for the future,” *Arch. Facial. Plast. Surg.* **3**, 207–213 (2001).
3. E. L. Schalow and A. J. Kirsch, “Laser tissue soldering: applications in the genitourinary system,” *Curr. Urol. Rep.* **4**, 56–59 (2003).
4. T. Menovsky, J. F. Beek, and S. L. Thomsen, “Laser(-assisted) nerve repair. A review,” *Neurosurg. Rev.* **18**, 225–235 (1995).
5. L. S. Bass and M. R. Treat, “Laser tissue welding: a comprehensive review of current and future clinical applications,” *Lasers Surg. Med.* **17**, 315–349 (1995).
6. B. Williams, N. R. Poulter, M. J. Brown, M. Davis, G. T. McInnes, J. F. Potter, P. S. Sever, and S. M. Thom, “British hypertension society guidelines for hypertension management 2004 (BHS-IV): summary,” *Br. Med. J. (Clin. Res. Ed)* **328**, 634–640 (2004).
7. V. L. Martinot, S. R. Mordon, V. A. Mitchell, P. N. Pellerin, and J. M. Brunetaud, “Determination of efficient parameters for argon laser-assisted anastomoses in rats: macroscopic, thermal, and histological evaluation,” *Lasers Surg. Med.* **15**, 168–175 (1994).
8. J. T. Tang, G. Godlewski, and S. Rouy, “Mechanism of aneurysm formation after 830-nm diode-laser-assisted microarterial anastomosis,” *J. Clin. Laser Med. Surg.* **15**, 175–179 (1997).
9. D. Pohl, L. S. Bass, R. Stewart, and D. T. Chiu, “Effect of optical temperature feedback control on patency in laser-soldered microvascular anastomosis,” *J. Reconstr. Microsurg* **14**, 23–29 (1998).
10. S. B. Self, D. A. Coe, and J. M. Seeger, “Limited thrombogenicity of low temperature, laser-welded vascular anastomoses,” *Lasers Surg. Med.* **18**, 241–247 (1996).
11. I. Kirman, A. Lauto, A. Phillips, A. Hamawy, E. Heldman, B. Cuomo, S. J. Shin, R. Soslow, D. Felsen, and D. P. Poppas, “Effect of laser welding with human serum albumin on the expression of P-selectin on platelets,” *Lasers Surg. Med.* **25**, 438–444 (1999).
12. K. M. McNally, B. S. Sorg, A. J. Welch, J. M. Dawes, and E. R. Owen, “Photothermal effects of laser tissue soldering,” *Phys. Med. Biol.* **44**, 983–1002 (1999).
13. K. M. McNally, B. S. Sorg, E. K. Chan, A. J. Welch, J. M. Dawes, and E. R. Owen, “Optimal parameters for laser tissue soldering. Part I: tensile strength and scanning electron microscopy analysis,” *Lasers Surg. Med.* **24**, 319–331 (1999).
14. D. Shumalinsky, L. Lobik, S. Cytron, M. Halpern, T. Vasilyev, A. Ravid, and A. Katzir, “Laparoscopic laser soldering for repair of ureteropelvic junction obstruction in the porcine model,” *J. Endourol* **18**, 177–181 (2004).
15. P. E. Grubbs Jr., S. Wang, C. Marini, S. Basu, D. M. Rose, and J. N. Cunningham Jr., “Enhancement of CO₂ laser microvascular anastomoses by fibrin glue,” *J. Surg. Res.* **45**, 112–119 (1988).
16. D. F. Cikrit, M. C. Dalsing, T. S. Weinstein, K. Palmer, S. G. Lalka, and J. L. Unthank, “CO₂-welded venous anastomosis: enhancement of weld strength with heterologous fibrin glue,” *Lasers Surg. Med.* **10**, 584–590 (1990).
17. G. S. Sica, N. Di Lorenzo, P. Sileri, and A. L. Gaspari, “Experimental microvascular anastomoses performed with CO₂, Argon, and Nd:YAG lasers,” *Ann. Ital. Chir.* **67**, 571–573 (1996).
18. S. Basu, S. Wang, R. Robertazzi, P. E. Grubbs, I. Jacobowitz, D. Rose, A. J. Acinapura, and J. N. Cunningham Jr., “In vitro bursting strength studies of laser-welded tissue and comparison with conventional anastomosis,” *J. Vasc. Surg.* **7**, 420–422 (1988).
19. P. J. Fahner, M. M. Idu, D. A. Legemate, E. Vanbavel, J. Borstlap, M. Pfaffendorf, J. van Marle, and T. M. van Gulik, “Morphological and functional alterations in glycerol preserved rat aortic allografts,” *Int. J. Artif. Organs* **27**, 979–989 (2004).
20. J. A. Kiernan, “Histological staining in one or two colours,” Chapter 6 in *Histological and Histochemical Methods. Theory and Practice*, 3rd ed, pp. 111–113, Arnold, New York (1999).
21. *Ibid.*, pp. 108–109.
22. E. V. Ross, J. R. McKinlay, and R. R. Anderson, “Why does carbon dioxide resurfacing work? A review,” *Arch. Dermatol.* **135**, 444–454 (1999).
23. E. V. Ross, G. S. Naseef, J. R. McKinlay, D. J. Barnette, M. Skrobal, J. Grevelink, and R. R. Anderson, “Comparison of carbon dioxide laser, erbium:YAG laser, dermabrasion, and dermatome: a study of thermal damage, wound contraction, and wound healing in a live pig

- model: implications for skin resurfacing," *J. Am. Acad. Dermatol.* **42**, 92–105 (2000).
24. K. J. Smith, H. G. Skelton, J. S. Graham, T. A. Hamilton, B. E. Hackley Jr, and C. G. Hurst, "Depth of morphologic skin damage and viability after one, two, and three passes of a high-energy, short-pulse CO₂ laser (Tru-Pulse) in pig skin," *J. Am. Acad. Dermatol.* **37**, 204–210 (1997).
 25. A. T. Yeh, B. Kao, W. G. Jung, Z. Chen, J. S. Nelson, and B. J. Tromberg, "Imaging wound healing using optical coherence tomography and multiphoton microscopy in an *in vitro* skin-equivalent tissue model," *J. Biomed. Opt.* **9**, 248–253 (2004).
 26. H. F. de Carvalho and S. R. Taboga, "The applicability of hematoxylin-eosin staining plus fluorescence or confocal laser scanning microscopy to the study of elastic fibers in cartilages," *C. R. Acad. Sci. III* **319**, 991–996 (1996).
 27. H. F. de Carvalho and S. R. Taboga, "Fluorescence and confocal laser scanning microscopy imaging of elastic fibers in hematoxylin-eosin stained sections," *Histochem. Cell Biol.* **106**, 587–592 (1996).
 28. M. R. Quigley, J. E. Bailes, H. C. Kwaan, L. J. Cerullo, J. T. Brown, and J. Fitzsimmons, "Comparison of bursting strength between suture- and laser-anastomosed vessels," *Microsurgery* **6**, 229–232 (1985).
 29. M. R. Quigley, J. E. Bailes, H. C. Kwaan, L. J. Cerullo, and J. T. Brown, "Aneurysm formation after low power carbon dioxide laser-assisted vascular anastomosis," *Neurosurgery* **18**, 292–299 (1986).
 30. J. Pearce and S. Thomsen, "Rate process analysis of thermal damage," Chapter 17 in *Optical-Thermal Response of Laser-Irradiated Tissue*, A. J. Welch and M. J. C. van Gemert, Eds., pp. 566–570, Plenum Press, New York (1995).
 31. <http://omlc.ogi.edu/spectra/water/index.html>.
 32. S. Wang, P. E. Grubbs Jr, S. Basu, R. R. Robertazzi, S. Thomsen, D. M. Rose, I. J. Jacobowitz, and J. N. Cunningham Jr., "Effect of blood bonding on bursting strength of laser-assisted microvascular anastomoses," *Microsurgery* **9**, 10–13 (1988).
 33. A. Lauto, "Repair strength dependence on solder protein concentration: a study in laser tissue-welding," *Lasers Surg. Med.* **22**, 120–125 (1998).
 34. J. Guo and Y. D. Chao, "Low power CO₂ laser-assisted microvascular anastomosis: an experimental study," *Neurosurgery* **22**, 540–543 (1988).
 35. B. H. Vale, A. Frenkel, S. Trenka-Benthin, and B. F. Matlaga, "Microsurgical anastomosis of rat carotid arteries with the CO₂ laser," *Plast. Reconstr. Surg.* **77**, 759–766 (1986).
 36. E. M. Ashworth, M. C. Dalsing, J. F. Olson, W. P. Hoagland, S. Baughman, and J. L. Glover, "Large-artery welding with a milliwatt carbon dioxide laser," *Arch. Surg. (Chicago)* **122**, 673–677 (1987).
 37. M. Okada, K. Shimizu, H. Ikuta, H. Horii, and K. Nakamura, "An alternative method of vascular anastomosis by laser: experimental and clinical study," *Lasers Surg. Med.* **7**, 240–248 (1987).
 38. S. Basu, C. P. Marini, M. S. Coons, T. T. Woloszyn, T. A. Folliguet, F. G. Baumann, and I. J. Jacobowitz, "Internal mammary coronary artery anastomosis by CO₂ laser: an acute experimental study," *J. Card. Surg.* **6**, 286–293 (1991).
 39. A. Ruiz-Razura, M. Lan, C. E. Hita, Z. Khan, N. H. Hwang, and B. E. Cohen, "Bursting strength in CO₂ laser-assisted microvascular anastomoses," *J. Reconstr Microsurg* **4**, 291–296 (1988).
 40. R. Schober, F. Ulrich, T. Sander, H. Durselen, and S. Hessel, "Laser-induced alteration of collagen substructure allows microsurgical tissue welding," *Science* **232**, 1421–1422 (1986).
 41. G. M. Lemole, R. R. Anderson, and S. DeCoste, "Preliminary evaluation of collagen as a component in the thermally induced 'weld'," *Proc. SPIE* **1422**, 116–122 (1991).
 42. N. T. Wright and J. D. Humphrey, "Denaturation of collagen via heating: an irreversible rate process," *Annu. Rev. Biomed. Eng.* **4**, 109–128 (2002).
 43. G. A. Pico, "Thermodynamic features of the thermal unfolding of human serum albumin," *Int. J. Biol. Macromol.* **20**, 63–73 (1997).
 44. B. Forer, T. Vasilev, Z. Gil, T. Brosh, N. Kariv, A. Katzir, and D. M. Fliss, "CO₂ laser fascia to dura soldering for pig dural defect reconstruction," *Skull Base* **17**, 17–23 (2007).
 45. D. Simhon, M. Halpern, T. Brosh, T. Vasilev, A. Ravid, T. Tennenbaum, Z. Nevo, and A. Katzir, "Immediate tight sealing of skin incisions using an innovative temperature-controlled laser soldering device: *in vivo* study in porcine skin," *Ann. Surg.* **245**, 206–213 (2007).
 46. D. Shumalinsky, L. Lobik, S. Cytron, M. Halpern, T. Vasilev, A. Ravid, and A. Katzir, "Laparoscopic soldering for repair of ureteropelvic junction obstruction in the porcine model," *J. Endourol* **18**, 177–181 (2004).